Comptes Rendus

Mécanique

Ran Xu, Enlong Liu and Huilin Xing

Analysis on mechanical properties and evolution of mesostructure of soil–rock mixture samples from contact network perspective

Short paper / *Note*

Analysis on mechanical properties and evolution of mesostructure of soil–rock mixture samples from contact network perspective

Ran Xu [a]**, Enlong Liu**[*, b, c] **and Huilin Xing** [d]

[a] Institute of Disaster Management and Reconstruction, Sichuan Univ., Chengdu 610207, China

[b] State Key Laboratory of Hydraulics and Mountain River Engineering, College of Water Resource and Hydropower, Sichuan Univ., Chengdu 610065, China

[c] Northwest Institute of Eco-Environment and Resources, State Key Laboratory of Frozen Soil Engineering, Chinese Academy of Sciences, Lanzhou 730000, China

[d] Earth Systems Science Computational Centre (ESSCC), The University of Queensland, St Lucia, Brisbane, QLD 4072, Australia

E-mails: 674958929@qq.com (R. Xu), liuenlong@scu.edu.cn (E. Liu), h.xing@uq.edu.au (H. Xing)

Abstract. Based on discrete element method (DEM), three kinds of soil–rock mixture (SRM) models with different coarse particle contents were established and triaxial compression tests were carried out. The results show that the force chains in the particle system playing the main bearing role need more lateral supports, which results in the contact with a higher coordination number and often bear larger contact force. The relationship between the contact's carrying capacity and the coordination number can be fit by a quadric surface. Taking the fit quadric surface as the capacity function, the network-flow model of force transfer can be constructed to quantify the force transfer ability of a contact network. By connecting the maximum flow in the network with the hardening parameter of the unified hardening model, the stress–strain relationship of SRM can be predicted to some extent, which lays a basis for formulating micro–macro constitutive model for granular materials.

Keywords. Granular material, Triaxial compression, Contact network, Critical state, Force chain.

---

[*] Corresponding author.

1. Introduction

As a kind of common geological material in nature, soil–rock mixture (SRM) is an important part of landslide and debris flow, so it is widely concerned. Since this kind of soil mass is composed of two kinds of materials, soil and rock, it is obviously different from ordinary soil in terms of mechanical properties and deformation characteristics. Previous studies have shown that the influence of rock content and rock shape on SRM mechanical properties, especially internal friction angle and cohesion, is particularly significant [1]. Although a large number of experiments have been conducted to explore the mechanical properties of SRM, few researches have been focused on analyzing the mesostructure evolution of SRM from the perspective of contact network. It is a popular method to analyze soil mesostructure evolution from the perspective of contact network [2, 3], which can provide the contact information between soil particles intuitively and reflect the evolution law [4]. This manuscript analyzes the mesoscopic evolution of SRM with different rock contents by the discrete element method (DEM) from the perspective of contact network, which can bridge the micro and macro parameters for granular materials and thus provide a basis for formulating a micro–macro constitutive model for soil.

For the SRM, many researchers have made achievements in experiment, theory and numerical simulation. Through large-scale direct shear tests, Xu *et al.* [1] found that in a certain range, with the increase of rock content, the shear strength and the size of shear zone of SRM would increase. Researchers analyzed the influence of rock content on the mechanical properties of samples from different perspectives. Yagiz *et al.* [5] believed that shear strength is mainly derived from the frictional forces developed due to sliding and interlock. Kokusho *et al.* [6] claimed that mechanical properties such as shear strength are affected by particle gradation. Vallejo [7] conducted static compaction tests on mixtures of two glass beads of different sizes (5 mm and 0.4 mm) to explore the effect of rock content on the mechanical properties of SRM. The results showed that when the coarse particle content is greater than 70%, the mixed structure is completely supported by coarse particles. When the coarse particle content is between 70% and 40%, the mixed structure is supported by both coarse and fine particles. When the coarse particle content is less than 40%, the structure of the mixture is completely supported by fine particles. Hamidi *et al.* [8] established a prediction equation for the shear strength of sand–gravel mixtures by considering the effect of particle crushing.

In recent years, numerical simulation has been becoming an important analysis method, which has more advantages in analyzing the local strain and many other aspects. Xu *et al.* [9] established a microstructural model of SRM by DIP-FEM based on image processing technology, and proposed three plastic zone development models of SRM. In order to further consider the influence of rock content on the mechanical properties of the SRM from the micro perspective, the DEM as a numerical simulation method is also used in the modeling of SRM. At present, there are two main methods to simulate SRM by discrete element. The first method is to conduct a three-dimensional discrete element modeling based on CT technology [10]. This method is relatively accurate but the modeling process is complex and the cost is high. The second method is the two-dimensional discrete element modeling based on Monte Carlo method [11]. Firstly, the spatial locations of rock fragments are generated uniformly, and then the size and azimuth angle are allocated to the corresponding location according to the certain rule (e.g., lognormal distribution principle). For the convenience of modeling and calculation, this study adopts the second method for modeling, assuming that the rock fragments are uniformly distributed.

As an analysis method, the contact network method often relies on the numerical simulation modeling of the discrete element, which is used to analyze the evolution of soil microstructure and the degree of particle rearrangement during the loading process. If soil is considered as granular material composed of soil particles, contact network formed by soil particle is undoubtedly

the simplest method to describe its properties, which is closely related to its mechanical features. According to the average contact force, Radjai *et al.* [12] divided the contact network into two sub-networks, strong network and weak network, and found that the strong network plays the main role of bearing force. Peters *et al.* [13] found that about half of the particles belonging to strong networks belong to force chains (a quasi-linear structure that transfers stronger forces in granular materials). Walker and Tordesillas [14, 15] analyzed the evolution of the meshes (they called it n-cycle, where n is the number of edges of the mesh, such as 3-cycle and 4-cycle) in the two-dimensional contact network. They found that the 3-cycle structure could inhibit the rotation of particles and affect the stability of the sample, and the 3-cycle structure with high contact force could provide an effective lateral support for the force chain. Tordesillas *et al.* [16] suggested that using MFMC algorithm to analyze the contact network can predict the force chain particles and the location of shear zone only according to the contact information without knowing the contact force. Therefore, the contact network method is helpful to analyze the complex failure mode and force transmission mode of SRM.

In this paper, the discrete element software Yade is employed to model rock–soil aggregate (RSA) with different rock contents, and the evolution of RSA in loading process is analyzed by the contact network method. In the process of modeling, RSA is simplified as a model composed of two kinds of grains, in which the fine grain represents soil and the coarse grain represents rock. In this study, the coarse grain content of the simulated samples is less than 40%, which makes the mechanical properties of the samples closer to the soil. This is because the contact force between two coarse particles is often much greater than other contact forces during the loading process, and when there are many coarse particles, there will be more contacts between the coarse particles, leading to a more complex contact network (the mixed structure is gradually supported by coarse particles [7]). According to the evolution of the contact network, the contact relationship and microstructure of RSA in the loading process are analyzed, and the flow network is established according to the coordination number of particles. The maximum flow of the flow network is introduced into the unified hardening model to predict the stress–strain relationship during the loading process.

2. The discrete element model of soil–rock mixture samples

Since the pioneering work of Cundall and Strack [17], DEM has been widely used to study different aspects of soil mechanics. Based on the basic constitutive relationships between interacting particles, DEM technology can provide the macroscopic response of particle assemblies under the variation of the external load. Each particle has its own mass, radius and moment of inertia. In each step of the calculation, the interaction between the particles and the resulting force on each particle are derived from the position of the particles by the law of interaction. Newton's second law is then integrated by explicit second-order finite difference scheme to calculate the new positions of the particles.

2.1. *Interparticle behavior*

The computing software used in this manuscript is Yade [18, 19]. In the process of calculating the contact force, the normal force F_n caused by the intergranular relative displacement in normal direction can be derived from the normal stiffness k_n. Similarly, the shear force F_t caused by the incremental tangential relative displacement can be derived from the tangential stiffness k_t and this tangential behavior conforms to the Coulomb friction law.

Table 1. DEM parameters

Parameter	Value
Number of particles	10,000
Sample height	0.03 m
Sample width	0.03 m
Particle diameter d	1.45 mm
Particle density ρ	2600 kg·m^{-3}
Normal spring stiffness k_n	5×10^7 N·m^{-1}
Shear spring stiffness k_s	2.5×10^7 N·m^{-1}
Damping coefficient	0.2
Loading strain rate	0.05 s^{-1}

2.2. *Modeling approach*

In the study of mechanical properties of SRM, the rock–soil threshold is a key parameter, which can be used to reasonably distinguish the rock and soil media in the mixture. In a certain scale of study, the particles whose sizes have a great impact on the failure mechanism and macroscopic mechanical properties of SRM are considered as "rocks," while the remaining particles are considered as "soil." Therefore, the concepts of "soil" and "rock" in SRM are relative, depending on the study scale. Medley *et al.* [1, 20] conducted a detailed study and proposed a criterion to distinguish the middle soil and rock in SRM based on the threshold value of soil and rock:

$$f = \begin{cases} R(d \geq d_{\text{thr}}) \\ S(d < d_{\text{thr}}), \end{cases} \tag{1}$$

where

$$d_{\text{thr}} = 0.05 L_c, \tag{2}$$

where R and S represent soil and "rock," respectively; d is the diameter of the particle; d_{thr} is the threshold of soil and rock; L_c is the characteristic engineering scale, which varies according to the working scale of the engineering problem under investigation. For the triaxial sample, L_c is equal to its diameter. The minimum size of rock fragments in this study is determined based on the above assumption.

In this study, the rock content of SRM is defined as the ratio between the mass of rock fragments and the total mass of the sample, that is, the mass ratio of coarse grain.

2.3. *Triaxial compression tests*

The modeling process based on DEM software Yade is shown as follows. Firstly, a sand sample model with random particle distribution is established. Secondly, the location and size of rock fragments are generated randomly according to the rock content. Finally, the particles within the range of each cuttings are combined with the clump command to represent each rock fragments.

The DEM numerical sample initially generated is composed of 10,000 spherical particles, the number of which is similar to that of Ju *et al.* [10] and He *et al.* [11]. The particle size is 1.45 mm, and the sample size is 30 mm × 30 mm × 30 mm. The relevant parameters of the initial generated samples are shown in Table 1.

The generation of the samples is mainly divided into two stages. In the first stage, all particles are placed uniformly within the range of the sample, and there is no contact or overlap between
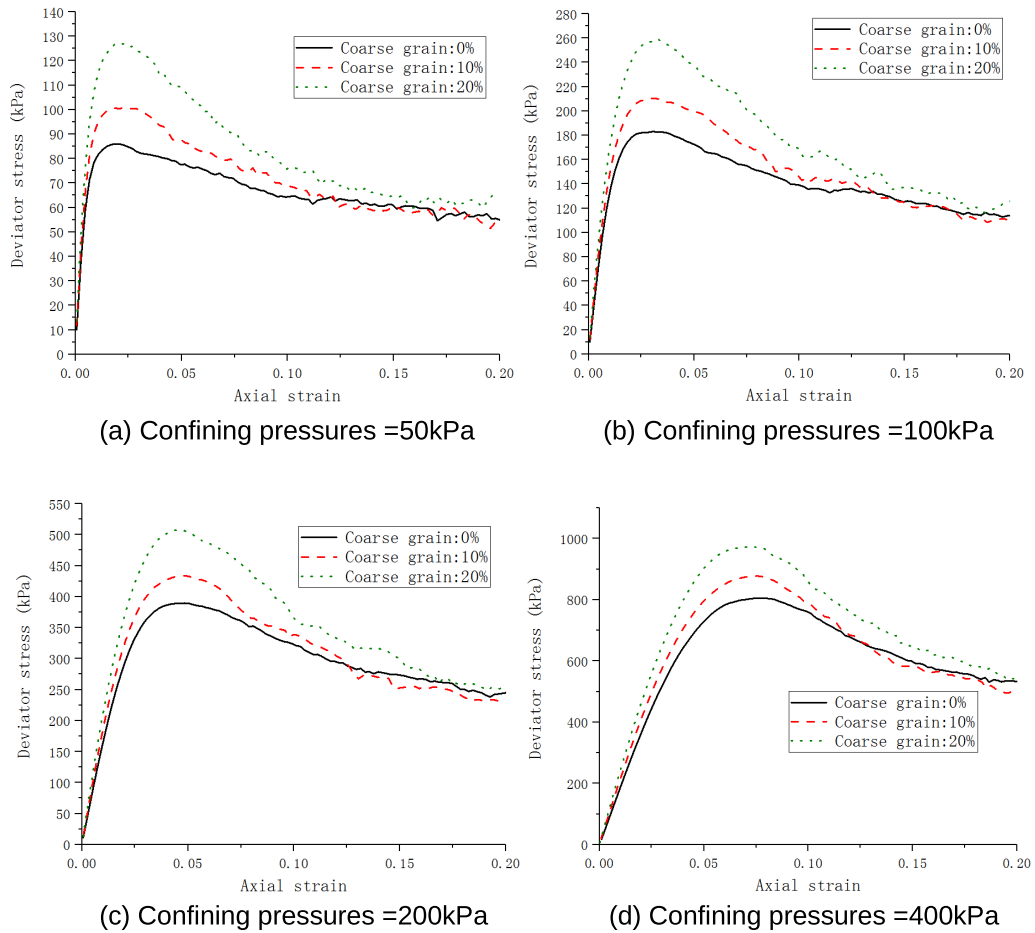
(a) Coarse grain: 0% (b) Coarse grain: 20%
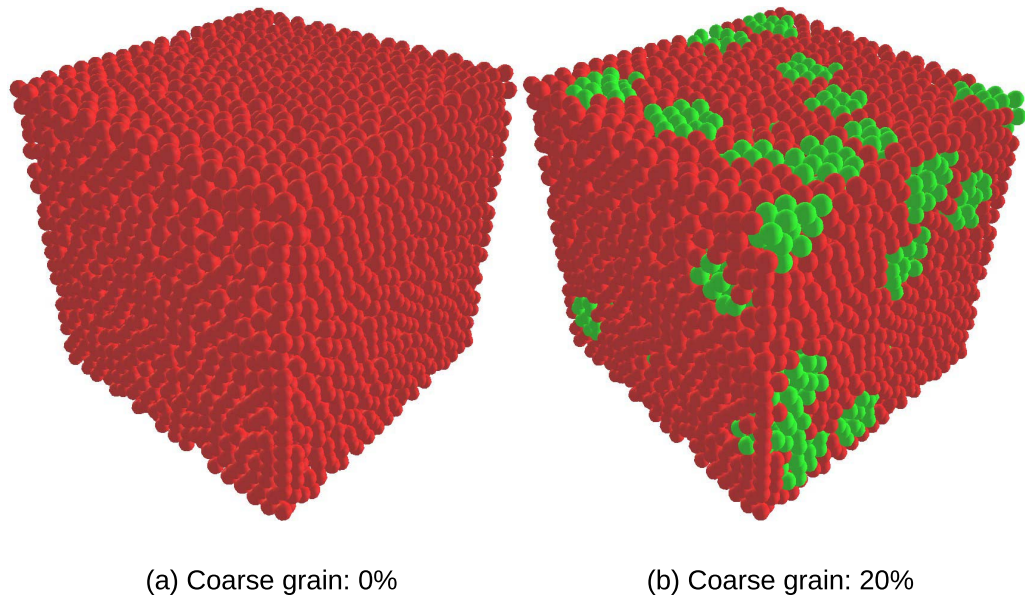
Figure 1. A view on aggregates (Axial strain = 0).

any two particles. The interparticle friction is set to 0 (to facilitate the generating of denser samples), and the particle radius is uniformly increased, during which the position of the boundary wall remains unchanged. This process continues until the porosity reaches 0.40. In the second stage, the interparticle friction is changed to 0.577 (equal to $\tan 30°$), so that the initial sample is generated. Then, according to the coarse grain content (in this study, 0%, 10%, and 20%), some of the particles are combined into rock fragments with the clump command, as shown in Figure 1 (the fine grain is red and the coarse grain is green). It is assumed that the rock fragments are approximately circular in shape, and their particle size is 4 mm. This treatment effectively reflects the relative irregularity of the rock fragments' surface.

In the triaxial compression tests of the numerical sample, isotropic compaction is firstly adopted to increase the confining pressure of the sample to the specified value (in this study, 50 kPa, 100 kPa, 200 kPa and 400 kPa). In order to ensure the homogeneity of loading and avoid the undesirable effects at the boundary, the loading plates adopt the frictionless rigid wall *et al.* [21]. The load is applied through the displacement of the wall, the loading strain rate in the Y-axis direction is constant and the stress in the X/Z direction is equal to the value of confining pressure. The loading strain rate is $0.05\,\text{s}^{-1}$, which satisfies the equation of quantifying the impact of inertia [22, 23] on the test, $I = \dot{\varepsilon} d \sqrt{\rho/p'} < 10^{-3}$ ($\dot{\varepsilon}$ is the strain rate, d the mean size of grains in the assembly, ρ the grain density and p' the mean effective stress). Therefore, the system can be considered to maintain quasistatic conditions during the loading process, where the inertial effect is negligible.

The evolution of the deviator stress and volume strain during loading is shown in Figures 2 and 3, respectively. Here, for more intuitive analysis, the compressive pressure and compressive strain are regarded as positive. It can be seen from the trend of the curve that the specimen shows strain softening behavior during the loading process, accompanied by the phenomenon of shear expansion. The peak shear strength increases with the confining pressure, and the dilatancy of the sample at failure decreases with the increase of confining pressure, which is qualitatively similar to the observation results of dense granular materials in laboratory experiments [24]. The

Figure 2. Deviator stress–axial strain curves at different confining pressures.

higher the coarse grain concentration, the higher the peak shear stress and the more obvious the dilatancy, which is similar to the results of other researchers [1, 7]. In the range of coarse grain concentrations in this study, the deviator stress of different samples under the same confining pressure in the critical state will reach the same level. This may be due to the larger disturbance of the coarse particles to the surrounding particles when they rotate and stagger during the loading process, resulting in greater dilatancy. In the early stage of loading, the main interaction between particles is occlusion, which makes the interaction between coarse and fine particles contribute more shear stress, leading to the increase of the peak shear stress with the increase of the coarse grain concentration. As the loading continues, the shear band may be gradually formed, and the interaction between particles is dominated by the sliding of particles in the shear band, while the sliding between particles is mainly controlled by the interparticle friction, so the shear stress will reach the same level in the critical state. For loose granular materials, the macro shear band is not often observed. In this paper, the simulated sample is medium-dense, in which all of them exhibit strain softening behavior and contraction followed by dilatancy. Of course, if the content of coarse grains is further increased (beyond the range of this study), there will be more sliding between coarse grains in the shear zone, which will greatly improve the shear stress level in the critical state, which is not intended to be discussed in this paper.
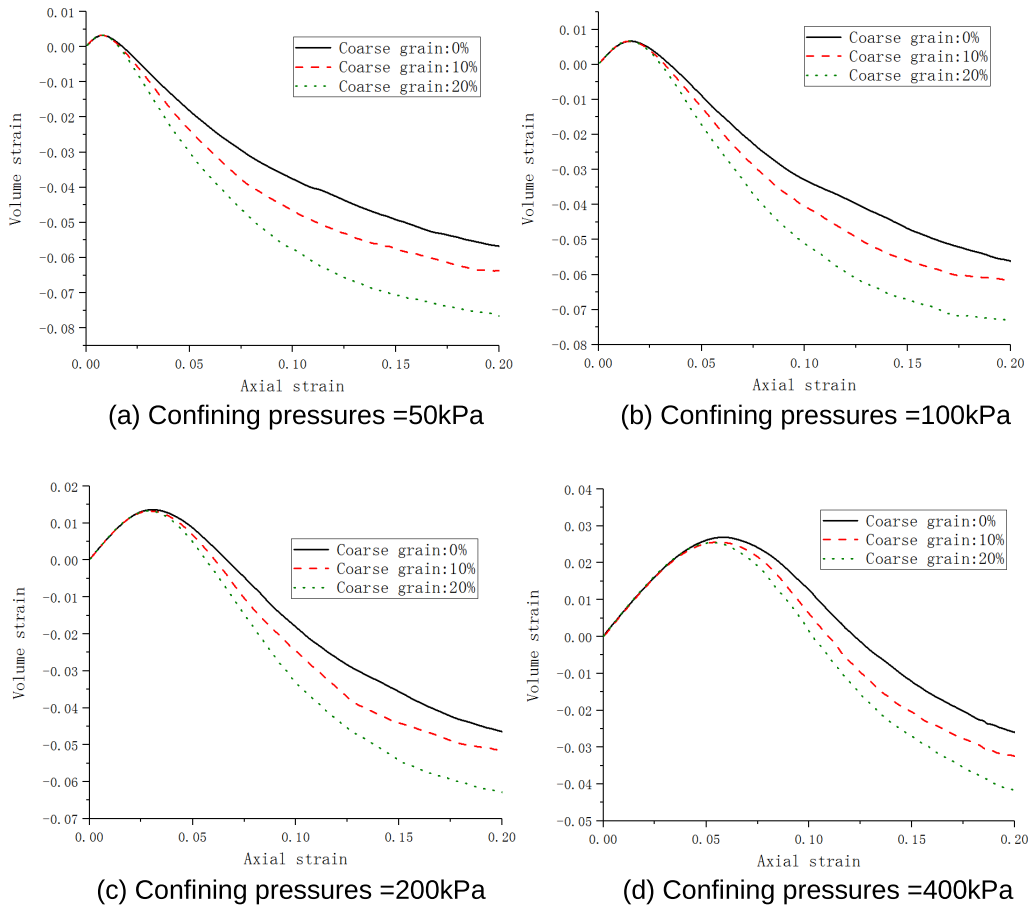
**Figure 3.** Volumetric strain–axial strain at different confining pressures.

3. Contact network analysis
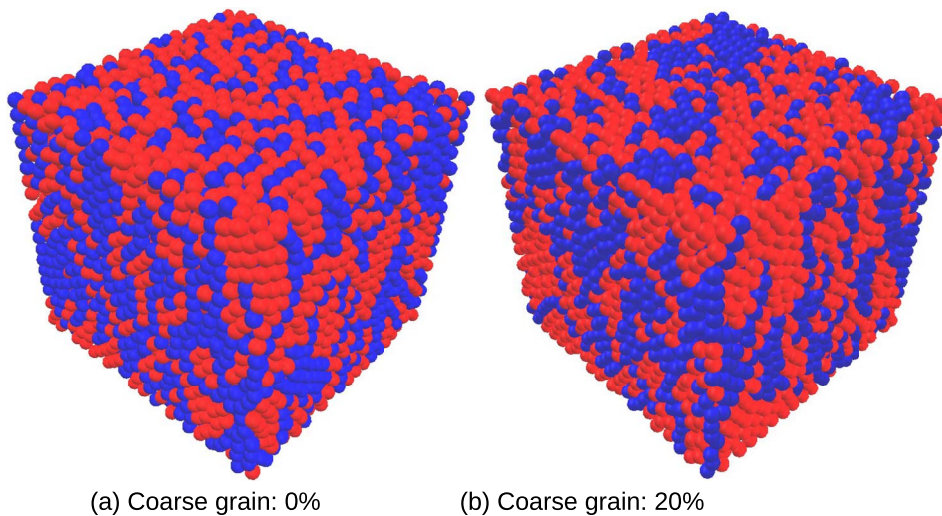
3.1. *Evolution of force chains*

In the particle system, the larger force is usually transferred along the path of the quasi-straight line, and a chain-like structure consisting of particles in this path is called a force chain *et al.* [13]. When the force chain structure buckles due to the axial compression, its axial load decreases as its particles move laterally. The description of the structure and evolution of the force chain is one of the core contents of granular material research. Many scholars have proposed their own methods to identify the force chain [13, 25]. In this paper, the force chain identification is based on the following criteria: the normal contact force is greater than the average value, the angle is less than 45° ($F_c > \overline{F}$, $\theta_c < 45°$), and the minimum number of grains to constitute a force chain is 3, as shown in Figure 4. Since the evolution trend of contact network is the same under different confining pressures [3], the following analysis takes the samples under 200 kPa confining pressure as example.

If the force chains are regarded as a force transmission structure in the granular material (Figure 5), then the evolution trend of the force transmission ability of the sample can be intuitively known through the statistics of their number, length and proportion of force chains (the proportion of the number of particles in the force chain to the total number of particles, and
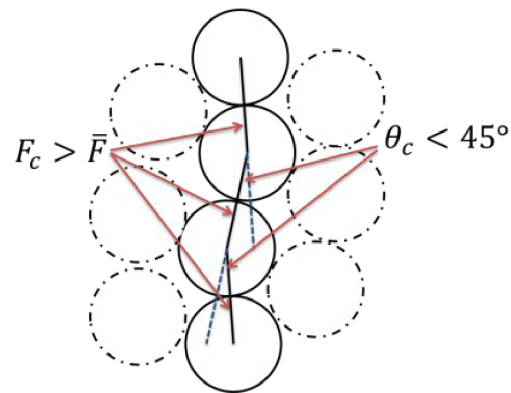
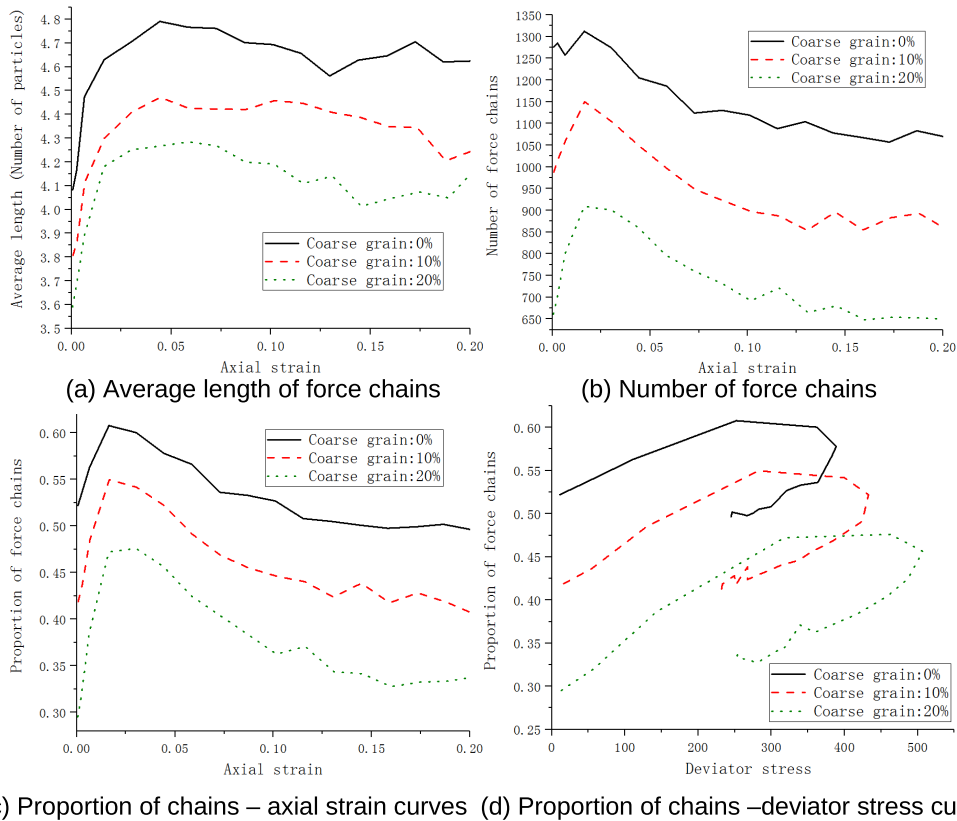**Figure 4.** Identification of force chains.

(a) Coarse grain: 0%   (b) Coarse grain: 20%

Figure 5. Distribution of force chains (blue particles) at peak deviator stress.

the total number of particles in the samples with different coarse grain contents are different). According to Figure 6(a, b, c), it can be seen that the number, length and proportion of force chains increase first, then decrease and finally tend to be stable. Figure 6(d) shows that in the initial stage, the force chain proportion increases with the increase of the deviator stress, then decreases slowly and finally decreases to the critical state with the decrease of the deviator stress. This is because the specimen is compacted in the early stage of loading, so that the force chains begin to grow. As the loading continues, the force chains gradually bear more external load, which makes the particles around them gradually unable to support them [26], so the force chains begin to buckle and destroy, and thus the shear band is produced [14]. When the shear zone is completely formed, the evolution of the force chain tends to be stable. The higher the coarse grain content, the lower the force chain proportion, which shows that coarse particles can transfer more force than fine particles, so many fine particles are replaced in the force chain. In addition, the proportion of force chains also affects the distribution of force chain length. Previous studies have shown that the distribution of the length of the force chain is approximately

(a) Average length of force chains   (b) Number of force chains

(c) Proportion of chains – axial strain curves   (d) Proportion of chains –deviator stress curves

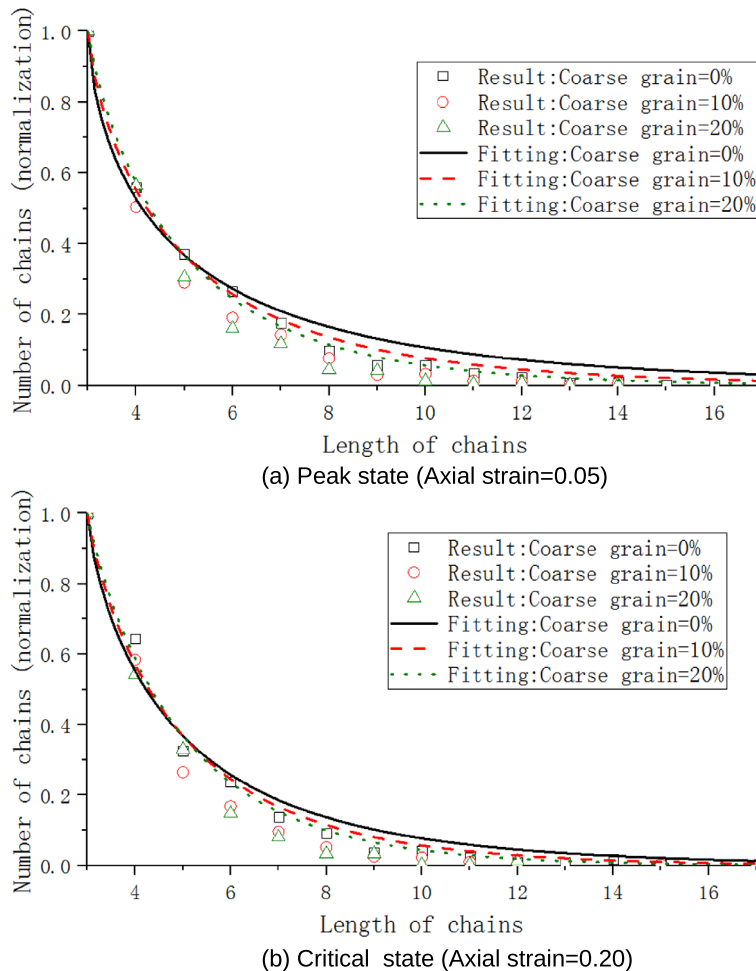**Figure 6.** Evolution of force chains.

exponential [27]. In this study, the distribution of the length of the force chain at each moment in the loading process can be fit by the following equation:

$$P(N) = e^{-((N-3)/A)^{1-RFC^A}}, \tag{3}$$

where RFC is the proportion of the particles belonging to the force chains in all particles, N is the length of the force chain (the number of particles on the force chain), $P(N)$ is the normalized value of the number of force chains and A depends on the search method of force chains and material properties (in this study, A is 2). In this treatment, it is assumed that the higher the RFC, the longer the force chains are likely to be generated in the particle system. The length distribution of the force chains at the moment when the deviator stress reaches its peak and at the moment of the critical state (when the axial strain reaches 0.20) is shown in Figure 7.

## 3.2. *Coordination number and contact force*

For granular materials, the contact network composed of the contact relationships between the particles can intuitively reflect the bearing capacities. In the contact network, each particle in the packing is represented as a node, and an edge exists between two particles if there is a contact (or many connects) between them. The process of particle rearrangement is the process of loss of old contact and formation of new contact in contact network. The coordination number of a node is equal to the number of edges attached to that node, and the coordination number of a contact

Figure 7. Length distribution of force chains.

network is equal to the average of the values of all nodes in this contact network. Coordination number is a convenient parameter of contact network, which can be used to represent the characteristics of the network, reflect the degree of particle rearrangement and the lateral support of the force chain.

It can be seen from Figure 8 that the overall trend of the coordination number evolution is a rapid decline after a short rise and finally, a gradual stabilization. The higher the coarse grain content, the lower the overall coordination number. The coordination number of the particles in the force chain is larger than that of other particles. This is because at the beginning of loading, the sample is compacted, and then with grain rearrangement and formation of shear band, a large number of contacts are broken until the sample is destroyed and the particles no longer have large-scale rearrangement. Because the force chain structure needs more lateral supports to ensure its stable force transmission, there will be more particles around the force chain particles. In the process of loading, when the coarse particles rotate and stagger, the disturbance to the surrounding particles is greater, and there are more particles around the coarse particles (see the subgraph in Figure 8(d)), so the coarse particles make the surrounding particles rearrange on a larger scale, thus making the overall coordination number drop faster.
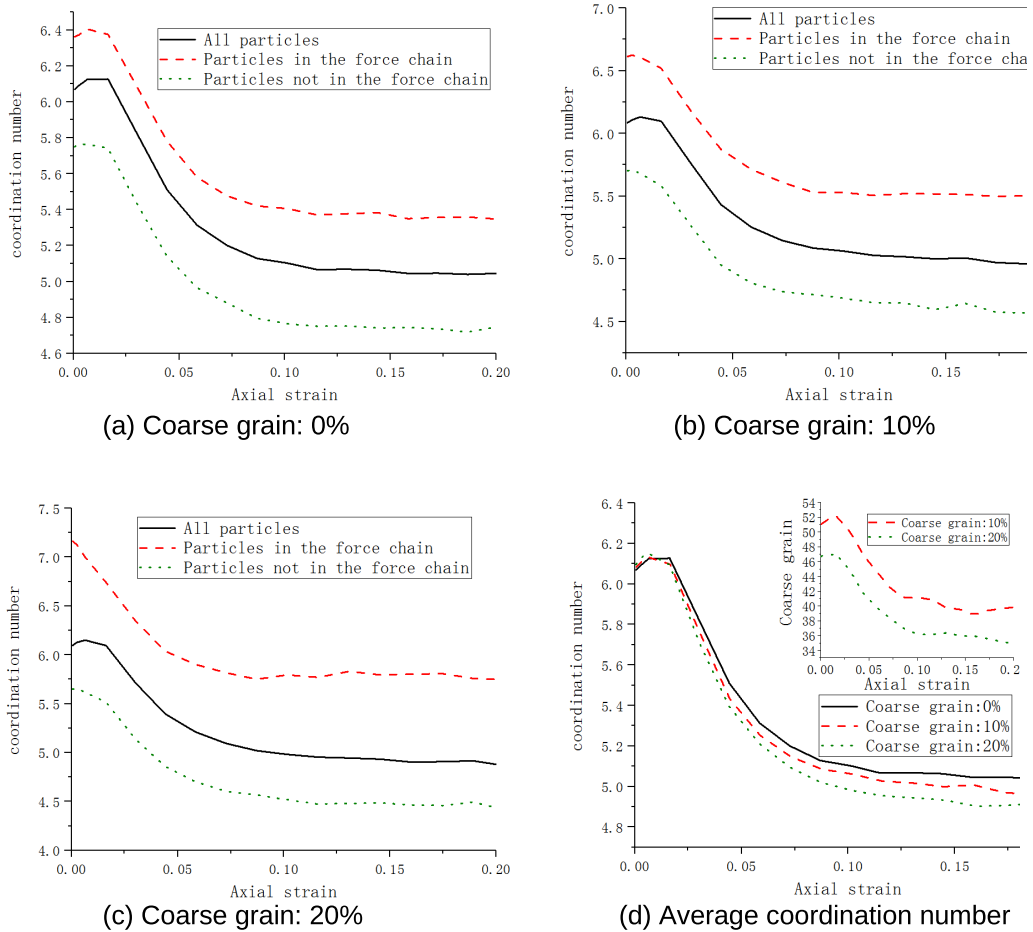
Figure 8. Evolution of coordination number.

According to the above analysis, the particles with a high coordination number are more likely to form force chains, and the force chains play an important supporting role in the whole particle system. This may indicate that the contact force of two particles with a higher coordination number is usually greater. In order to explore the relationship between the coordination number and the contact force, we counted all the contact forces at the moment of the peak state (axial strain = 0.05), and classified them according to the coordination number of the two particles making up the contact, and tried to take the average value for each type of contact. We find that the quadric surface fit by the least square method can reflect the relationship between the coordination number and the average value of each kind of contact force, as shown in Figure 9 (Z_1, Z_2 are the coordination number of the two particles, fn is the average normal contact force). The fitting function is expressed as follows:

$$fn = AZ_1^2 + BZ_1Z_2 + AZ_2^2 + CZ_1 + CZ_2 + D, \tag{4}$$

where A, B, C, D are the fitting parameters, which are related to the coarse grain content in this study (when the coarse grain content is 0, $A = -0.0167, B = -0.0003, C = 0.2199, D = -0.7326$; when the coarse grain content is 10%, $A = -0.0008, B = 0.0006, C = 0.0735, D = -0.1454$; when the coarse grain content is 20%, $A = -0.0019, B = 0.0014, C = 0.1239, D = -0.6295$). When

(a) Coarse grain: 0%   (b) Coarse grain: 20%
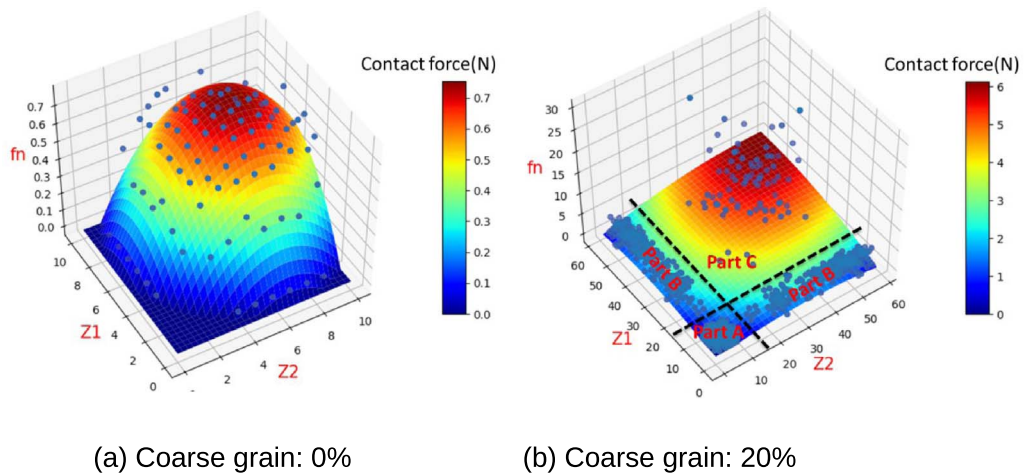
Figure 9. Distribution of contact forces at peak deviator stress.

the calculation result is less than zero, the fitting value is equal to zero, because this study assumes that the contact force between particles does not include tension. The significance of this treatment is to show that if the maximum allowable contact force of the contact is related to the coordination number of the two particles, only when the coordination numbers of both particles are high can the contact have the possibility of generating larger contact force. It can be seen from the corresponding relationship between the function (curved surface) and the simulation results (scattered points) in Figure 9 that the fitting effect is better when the coarse grain content is 0%. When the content of coarse particles is 20%, Equation (4) can better fit the contact force between fine particles and fine particles (Part A) and the contact force between fine particles and coarse particles (Part B), but it will significantly underestimate the contact force between coarse particles and coarse particles (Part C). Therefore, this method can only be used to estimate the situation when the coarse grain content is small. When the coarse grain content is high, the contact between coarse particles will be more, which will make the fitting more inaccurate.

3.3. *Network-flow model of force transfer*

In order to connect the force transfer ability of the contact network with the macroscopic mechanical response of the specimen, it is a good choice to establish a network-flow model for force transfer. At present, the main applications of the network-flow model of force transfer are as follows: to locate the position of shear band with maximum-flow–minimum-cut [28], and to predict the formation of force chains with maximum-flow–minimum-cost (MFMC) [29]. The flow network is composed of a source node, a sink node, intermediate nodes and edges. In the flow network, the flow transfers from the source to the sink along the edges and passes through intermediate nodes. Each edge in the flow network has its own capacity, which indicates the maximum flow that the edge is allowed to pass through. If the flow is regarded as the contact force transmitted in the particle system, the network-flow models of force transmission in granular material can be established. The steps for establishing a network-flow model for force transfer are shown in Figure 10. According to the distribution of the force chains, the transfer of larger contact forces is mainly along the direction of principal stress. Therefore, it is assumed that the top wall and bottom wall are the source and sink, the particles are the intermediate nodes, and the

(a) Particle packing and walls

(b) Contact network and walls

(c) Flow network

(d) Maximum flow
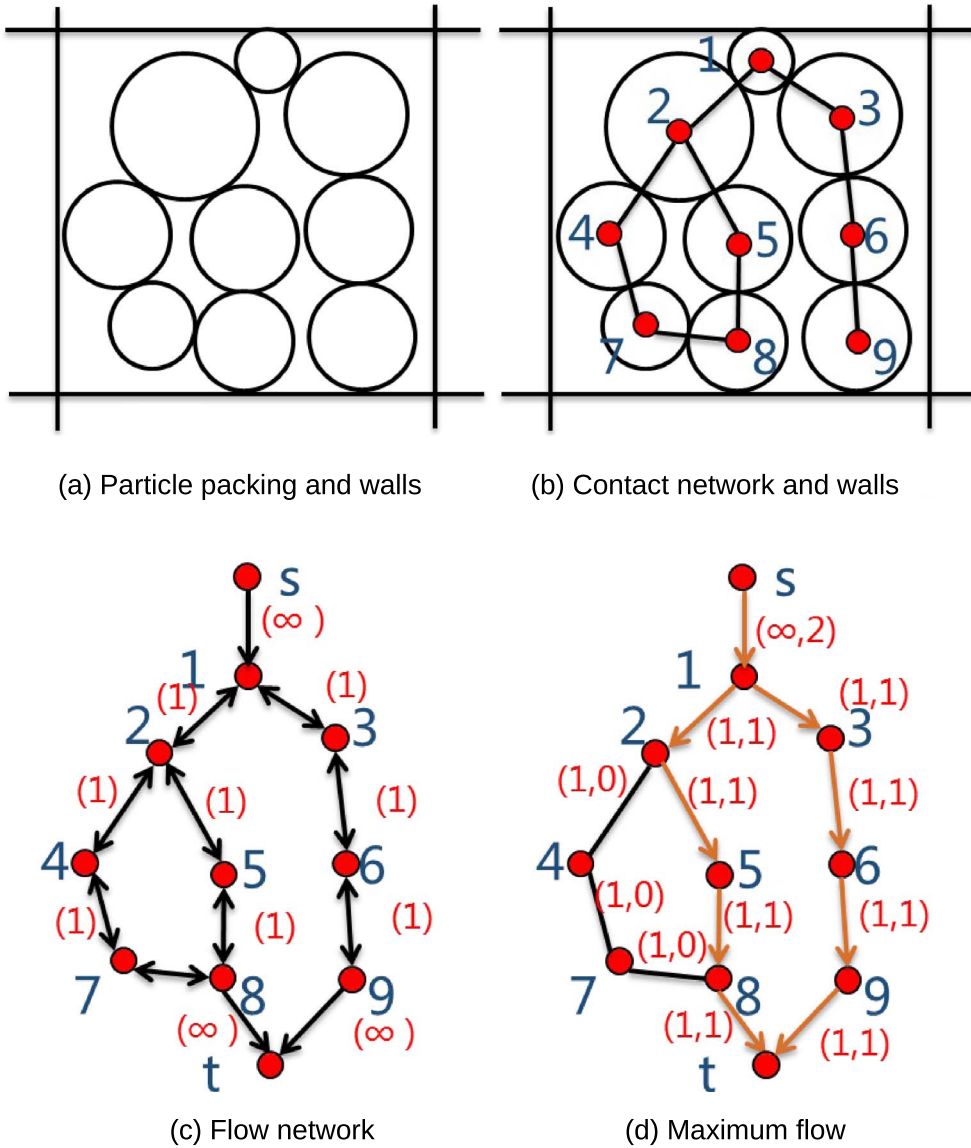
Figure 10. The network-flow models of force transmission.

flow is the force transferred from the top wall to the bottom wall. The contacts between particles or between particle and wall is defined as the edges in the flow network. The capacity of the edge represents the maximum contact force that can be carried by the contact. It is defined that the transfer of flow between particles can be two-fold, but the transfer of flow between particle and wall is one-way (it can only be transferred from the source to the intermediate node, or from the intermediate node to the sink), and the inflow flow at each intermediate node is equal to the outflow flow. This reflects the balance of forces on each particle, and the external force is inputted into the particle system through the loading plates. As the force on the loading plate is artificially loaded, the capacity between the wall and particles is regarded as infinite, and the capacity between particles depends on the property of the contact. In the example of Figure 10,
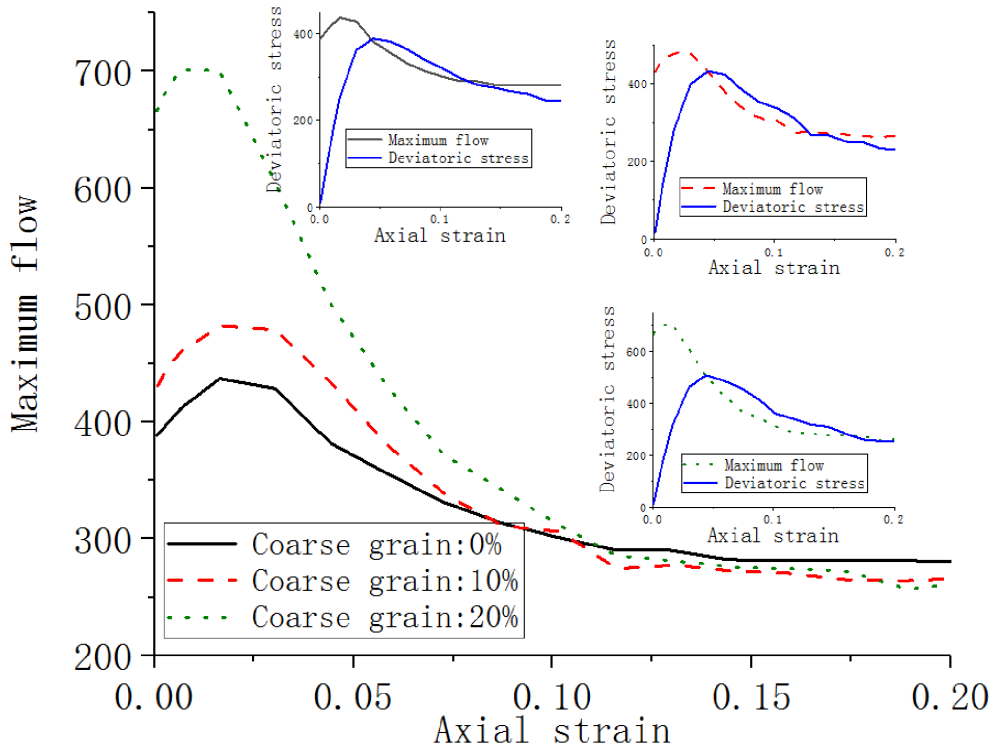
Figure 11. Evolution of maximum flow.

we assume that the maximum contact force (capacity) between each particle is 1, as shown in Figure 10(c). By solving the maximum network flow, we can get the maximum flow scheme shown in Figure 10(d). The calculation method can be referred to reference [30]. From Figure 10(d), it can be seen that the maximum flow through the network is 2, and a scheme of flow distribution is also given (the yellow path is the flow path, the second number in brackets is the flow size and the first is the capacity).

Determining the reasonable capacity for each edge is the key to the effective use of network-flow model of force transfer, which requires the construction of a reasonable capacity function. According to the previous content, we assume that the capacity function is related to the coordination number, which is (4). It is assumed that when the sample is in the peak state, each contact reaches its best state. It is found that if (4) obtained by fitting the average value of 1.4 times of the contact forces in the peak state is taken as the capacity function, then the maximum flow at this time is almost equal to σ_1 (forces on upper and lower loading plates, i.e., the maximal principal stress of the specimen). The capacity function of each sample can be obtained by fitting each sample according to the contact force distribution of the peak state. According to the capacity function, the maximum flow of the sample at each time during the loading process is calculated. In order to better compare the maximum flow with the macroscopic mechanical response of the samples, we subtract the confining pressure from the value of the maximum flow and divide it by the area of the loading plate, so that the new maximum flow and deviator stress are the same dimension, as shown in Figure 11.

It can be seen from the figure that the curve trend of the maximum flow is that after a short rise, the maximum flow decreases rapidly and finally reaches a stable state. In the initial state,

the value of the maximum flow increases with the increase of the coarse grain content, but they will eventually reach the same stable state. The relationship between the deviator stress and the maximum flow can be divided into three stages: before reaching the peak state, the deviator stress is lower than the maximum flow; after reaching the peak state, the deviator stress gradually decreases until it is lower than the maximum flow; and after the maximum flow reaches the stable value, the deviator stress gradually tends to be stable. This shows that the maximum flow is a specific quantification of the force transfer ability of the particle system. As mentioned above, the force transfer ability of the sample changes with the evolution of the force transfer structure of force chain, while the sample with a high coarse grain content has stronger force transfer ability in the initial state, and all the samples have the same force transfer ability in the critical state. The distribution of force in particle system always tends to reach the best state of force transmission, so the deviator stress increases continuously at the initial state to approach the maximum flow. After the peak state, because the deviator stress of the system exceeds the capacity of the network-flow model of force transfer, it begins to show the trend of strain softening, and finally reaches a stable value with the maximum flow.

4. Maximum flow and unified hardening model

In the past, the network-flow model of force transfer mostly predicted the position of shear band and paths of force chains through the contact relationship between particles, but it was rarely used to predict the stress–strain relationship during the loading process. This study attempts to apply the maximum flow to the unified hardening model and further explore the practicability of the network-flow model of force transfer. By using the new hardening parameter H to replace the hardening parameter in the modified Cam-clay model [31, 32], i.e., the plastic volume strain, Yao *et al.* [33, 34] revised the modified Cam-clay model which can describe the shear contraction followed by dilatancy, which is called the unified hardening model.

4.1. *Unified hardening parameter H*

For dense sand, the hardening parameters of the unified hardening model can be expressed as follows [33, 34]:

$$H = \int \mathrm{d}H = \int \frac{M_f^4 - \eta^4}{M^4 - \eta^4} \mathrm{d}\varepsilon_v^p, \tag{5}$$

where M is the critical state stress ratio, η ($\eta = q/p$, q is the deviatoric stress, p is the mean principal stress) is the stress ratio, ε_v^p is the plastic volume strain and M_f is the potential strength. The potential failure stress ratio M_f is introduced to characterize the potential ability of the sample to resist shear failure under current conditions. Based on different assumptions, M_f has different calculation methods. In this study, we consider that the potential strength is related to the force transfer ability of the contact network, i.e., $M_f = F_{\max}/p$, $F_{\max}$ is the maximum flow of the network-flow model of force transfer.

The relationship between M_f, η, and M in the loading process of the sample is shown in Figure 12. The different relationships between them indicates the different stages in the loading process:

(1) In strain hardening state ($\mathrm{d}H > 0$)
   (a) When $0 < \eta < M$, $\mathrm{d}\varepsilon_v^p > 0$, the sample is in a state of contraction.
   (b) When $\eta = M$, $\mathrm{d}\varepsilon_v^p = 0$, the sample is in the boundary between the state of contraction and the state of dilatancy.
   (c) When $M < \eta < M_f$, $\mathrm{d}\varepsilon_v^p < 0$, the sample is in a state of dilatancy.
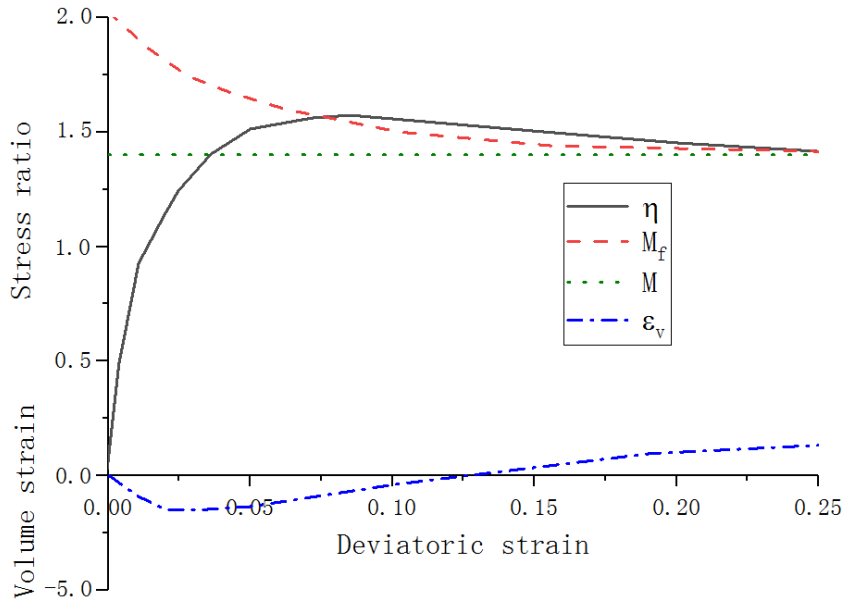
Figure 12. Potential failure stress ratio M_f, stress ratio η (= q/p), critical state stress ratio M and volumetric strain ε_v against deviatoric strain ε_d.

(2) In peak state ($dH = 0$)
   When $\eta = M_f$, the potential strength is equal to the peak strength, and the sample changes from strain hardening state to strain softening state.
(3) In strain softening state ($dH < 0$)

Since $dH < 0$, $\eta > M$ and η is slightly higher than M_f, $d\varepsilon_v^p < 0$, which indicates contraction. When the sample reaches the critical state, $\eta = M = M_f$ and $d\varepsilon_v^p = dH = 0$.

4.2. *Elastoplastic constitutive relation in p–q space*

The yield surface assumption is similar to the modified Cam-clay model, and the associated flow rule is adopted, as shown in (6), (7). The hardening parameter H [33] is shown in (5). Equation (7) is the result obtained after the hardening parameter H is substituted into (6). Equation (6) can also represent the yield function of the modified Cam-clay model. Equations (6) and (7) indicate that the unified hardening model is based on the modification of the modified Cam-clay model.

$$f = g = \ln \frac{p}{p_x} + \ln \left(1 + \frac{q^2}{M^2 p^2}\right) = 0 \tag{6}$$

$$f = \ln \frac{p}{p_{x0}} + \ln \left(1 + \frac{q^2}{M^2 p^2}\right) - \frac{1}{c_p} H = 0, \tag{7}$$

where p_x is the intersection of the yield surface with the p-axis; p_{x0} is the initial value of p_x with $\varepsilon_v^p = 0$ and $H = 0$; $c_p = (\lambda - \kappa)/(1 + e_0)$; λ is the slope of the normal compression line; κ is the slope of the unloading line and e_0 is the initial void ratio.

According to the above equation, the constitutive relation of the unified hardening model in p–q space can be expressed as follows:

$$\left\{ \begin{array}{c} \mathrm{d}p \\ \mathrm{d}q \end{array} \right\} = \left[\begin{array}{cc} C_{pp} & C_{pq} \\ C_{pq} & C_{qq} \end{array} \right] \left\{ \begin{array}{c} \mathrm{d}\varepsilon_v \\ \mathrm{d}\varepsilon_d \end{array} \right\} \tag{8}$$

$$\begin{cases} C_{pp} = \dfrac{K((M_f^4 - \eta^4)p + 12Gc_p\eta^2)}{(M_f^4 - \eta^4)p + 12Gc_p\eta^2 + Kc_p(M^2 - \eta^2)^2} \\[4mm] C_{pq} = \dfrac{3KG(-2c_p(M^2 - \eta^2)\eta)}{(M_f^4 - \eta^4)p + 12Gc_p\eta^2 + Kc_p(M^2 - \eta^2)^2} \\[4mm] C_{qq} = \dfrac{3G((M_f^4 - \eta^4)p + Kc_p(M^2 - \eta^2)^2)}{(M_f^4 - \eta^4)p + 12Gc_p\eta^2 + Kc_p(M^2 - \eta^2)^2} \end{cases} \tag{9}$$

$$K = E/[3(1 - 2\nu)] \tag{10}$$

$$G = E/[2(1 + \nu)] \tag{11}$$

$$E = 3p(1 - 2\nu)(1 + e_0)/\kappa, \tag{12}$$

where K and G are the elastic bulk modulus and the elastic shear modulus, respectively; E is the elastic modulus and ν is Poisson's ratio. Potential strength M_f is related to the force transfer ability of the contact network, i.e., $M_f = F_{\max}/p$, $F_{\max}$ is the maximum flow of the network-flow model of force transfer (obtained from Section 3.3). When $M_f = M$, Equation (9) is the same as that in modified Cam-clay model.

4.3. *Prediction and verification of the model*

Ishihara *et al.* [35, 36] conducted a large number of triaxial tests on Toyoura sand, and the test results have been used by many scholars to verify its constitutive model. According to this, Yao *et al.* [37] adopted the corresponding model parameters in the study of unified hardening model of sand. In this paper, the stress–strain relationship of contact network is only used for primary discussion, so the selection of relevant parameters is also in accordance with this (the slope of the normal compression line λ is 0.135; the slope of the unloading line κ is 0.04; Poisson's ratio ν is 0.3). The critical state stress ratio M is set as 0.8 according to DEM simulation results.

According to the selection of parameters and the previous contact network analysis, the comparison between simulated values of three samples with different coarse grain concentrations under 200 kPa is shown in Figure 13. The results show that the unified hardening model considering the maximum flow can roughly reflect the tendency of the deviator stress and volume strain of the samples with different coarse grain contents during loading. In general, the model can reflect the trend of the deviator stress and volume change with the different coarse grain concentrations: the higher the coarse grain content, the higher the peak value of deviator stress, the more obvious the phenomenon of dilatancy, but when the critical state is reached, the deviator stress values of all samples are equal. This shows that the force transfer ability of the sample reflected by the network-flow model of force transfer can be used to explain the stress–strain relationship of the sample in the loading process to a certain extent.

5. Conclusions

In summary, this study investigated the macroscopic mechanical behavior of SRM with different rock contents and confining pressures under triaxial compression loading path, and established a connection between macroscopic and microscopic through contact network. The conclusions
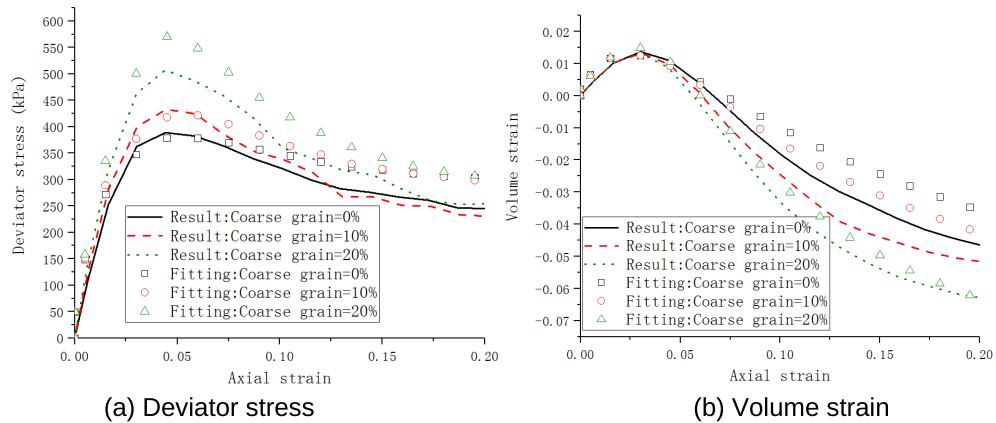
Figure 13. Simulation and fitting values of deviator stress and volume strain.

are summarized as follows (it is worth noting that for reasons of length, this paper only considers the case of triaxial compression loading path).

(1) The results of DEM numerical simulation show that the samples with 0%, 10% and 20% coarse particles have different mechanical behaviors under the same confining pressure. The higher the coarse grain content, the higher the peak shear stress and the more obvious the dilatancy. In the critical state, all specimens reach the same deviator stress level.

(2) The evolution of the force chains can reflect the change of the force transfer ability of the particle system. The number, length and proportion of force chains increase first, then decrease, and finally tend to be stable. The higher the coarse grain contact, the lower the force chain proportion. In addition, the proportion of force chains also affects the distribution of force chain length.

(3) The particles with a high coordination number are more likely to form force chains, and the contact force of two particles with a higher coordination number is usually greater. The quadric surface fit by the least square method can reflect the relationship between the coordination number and the average value of each kind of contact force, but this method is only suitable for the case of low coarse grain content.

(4) Taking the relationship between the contact force and coordination number as a capacity function, the network-flow model of force transfer can be constructed to quantify the force transfer ability of contact network. By connecting the maximum flow in network flow with the unified hardening model, the stress–strain relationship of SRM can be predicted relatively well to some extent.

Conflicts of interest

The authors declare that there are no conflicts of interest regarding the publication of this paper.

Acknowledgements

References

[1] X. Wen-Jie, X. Qiang, H. Rui-Lin, "Study on the shear strength of soil–rock mixture by large scale direct shear test", *Int. J. Rock Mech. Min. Sci.* **48** (2011), no. 8, p. 1235-1247.

[2] J. Tian, E. Liu, L. Jiang, X. Jiang, Y. Sun, R. Xu, "Influence of particle shape on the microstructure evolution and the mechanical properties of granular materials", *C. R. Méc.* **346** (2018), no. 6, p. 460-476.

[3] J. Xiaoqiong, L. Enlong, J. Lian *et al.*, "Evolution of meso-structures and mechanical properties of granular materials under triaxial compression state fromcomplex network perspective", *Granul. Matter* **20** (2018), no. 3, article no. 54.

[4] J. Lian, L. Enlong, T. Jianqiu *et al.*, "Effects of inter-particle frictional coefficients on evolution of contact networks in landslide process", *Engineering* **9** (2017), p. 917-936.

[5] S. Yagiz, "Brief note on the influence of shape and percentage of gravel on the shear strength of sand and gravel mixtures", *Bull. Eng. Geol. Environ.* **60** (2001), no. 4, p. 321-323.

[6] T. Kokusho, T. Hara, R. Hiraoka, "Undrained shear strength of granular soils with different particle gradations", *J. Geotech. Geoenviron. Eng.* **130** (2004), no. 6, p. 621-629.

[7] L. E. Vallejo, "Interpretation of the limits in shear strength in binary granular mixtures", *Can. Geotech. J.* **38** (2001), no. 5, p. 1097-1104.

[8] A. Hamidi, M. Alizadeh, S. M. Soleimani, "Effect of particle crushing on shear strength and dilation characteristics of sand-gravel mixtures", *Int J. Civil Eng.* **7** (2009), no. 1, p. 61-71.

[9] W. J. Xu, Z. Q. Yue, R. L. Hu, "Study on the mesostructure and mesomechanical characteristics of the soil–rock mixture using digital image processing based finite element method", *Int. J. Rock Mech. Min. Sci.* **45** (2008), no. 5, p. 749-762.

[10] Y. Ju, H. F. Sun, M. X. Xing, X. F. Wang, J. T. Zheng, "Numerical analysis of the failure process of soil–rock mixtures through computed tomography and PFC3D models", *Int. J. Coal Sci. Technol.* **5** (2018), no. 2, p. 126-141.

[11] J. He, X. Li, S.-D. Li, J.-L. Gu, "Numerical study of rock–soil aggregate by discrete element modeling", in *Sixth International Conference on Fuzzy Systems and Knowledge Discovery*, IEEE, 2009, p. 565-569.

[12] F. Radjai, D. E. Wolf, M. Jean *et al.*, "Bimodal character of stress transmission in granular packings", *Phys. Rev. Lett.* **80** (1998), no. 1, p. 61-64.

[13] J. F. Peters, M. Muthuswamy, J. Wibowo *et al.*, "Characterization of force chains in granular material", *Phys. Rev. E* **72** (2005), no. 4, article no. 041307.

[14] A. Tordesillas, D. M. Walker, Q. Lin, "Force cycles and force chains", *Phys. Rev. E* **81** (2010), no. 1, article no. 011302.

[15] D. M. Walker, A. Tordesllas, "Topological evolution in dense granularmaterials:a complex networks perspective", *Int. J. Solids Struct.* **47** (2010), no. 5, p. 624-639.

[16] A. Tordesillas, S. T. Tobin, M. Cil *et al.*, "Network flow model of force transmission in unbonded and bonded granular media", *Phys. Rev. E* **91** (2015), no. 6, article no. 062204.

[17] P. A. Cundall, O. D. L. Strack, "Discussion: A discrete numerical model for granular assemblies", *Géotechnique* **30** (1980), no. 3, p. 331-336.

[18] J. Kozicki, F. V. Donze, "YADE-OPEN DEM: an open-source software using a discrete element method to simulate granular material", *Eng. Comput.* **26** (2009), no. 7-8, p. 786-805.

[19] J. Kozicki, F. V. Donze, "A new open-source software developed for numerical simulations using discrete modeling methods", *Comput. Methods Appl. Mech. Eng.* **197** (2008), no. 49-50, p. 4429-4443.

[20] E. Medley, E. S. Lindquist, "The engineering significance of the scale-independence of some Franciscan mélanges in California", in *USA 35th U. S. Symposium*, 1995, p. 907-914.

[21] L. Scholtes, B. Chareyre, F. Nicot *et al.*, "Micromechanics of granular materials with capillary effects", *Int. J. Eng. Sci.* **47** (2009), no. 1, p. 64-75.

[22] F. da Cruz, S. Emam, M. Prochnow *et al.*, "Rheophysics of dense granular materials: Discrete simulation of plane shear flows", *Phys. Rev. E* **72** (2005), no. 2, article no. 021309.

[23] J. C. Lopera Perez, C. Y. Kwok, C. OŒSullivan *et al.*, "Assessing the quasi-static conditions for shearing in granular media within the critical state soil mechanics framework", *Soils Found.* **56** (2016), p. 152-159.

[24] G. Yan, H. S. Yu, G. Mcdowell, "Simulation of granular material behaviour using DEM", *Proc. Earth Planet. Sci.* **1** (2009), no. 1, p. 598-605.

[25] S. Qi-cheng, X. Hai-li, L. Jian-guo, J. Feng, "Skeleton and force chain network in static granular material", *Rock Soil Mech.* **30** (2009), p. 83-87.

[26] H. Zhu, F. Nicot, F. Darve, "Meso-structure organization in two-dimensional granular materials along biaxial loading path", *Int. J. Solids Struct.* **96** (2016), p. 25-37.

[27] L. Zhang, Y. J. Wang, J. Zhang, "Force-chain distributions in granular systems", *Phys. Rev. E* **89** (2014), no. 1, article no. 012203.

[28] A. Tordesillas, A. Cramer, D. M. Walker, "Minimum cut and shear bands", *AIP Conf. Proc.* **1542** (2013), no. 1, p. 507-510.

[29] Q. Lin, A. Tordesillas, "Towards an optimization theory for deforming dense granular materials: Minimum cost maximum flow solutions", *J. Ind. Manag. Optim.* **10** (2014), no. 1, p. 337-362.

[30] R. K. Ahuja, T. L. Magnanti, J. B. Orlin, "Network flows: theory, algorithms and applications", *J. Oper. Res. Soc.* **45** (1993), no. 11, p. 791-796.

[31] K. H. Roscoe, A. Thurairajah, A. N. Schofield, "Yielding of clays in states wetter than critical", *Géotechnique* **13** (1963), no. 3, p. 211-240.

[32] K. H. Roscoe, A. N. Burland, in *On the Generalized Behaviour of "Wet" Clay* (J. Heyman, F. Leckie, eds.), Cambridge University Press, London, 1968, p. 535-609.

[33] Y. P. Yao, W. Hou, A. N. Zhou, "UH model: three-dimensional unified hardening model for overconsolidated clays", *Geotechnique* **59** (2009), no. 5, p. 451-469.

[34] Y. P. Yao, D. A. Sun, T. Luo, "A critical state model for sands dependent on stress and density", *Int. J. Numer. Anal. Meth. Geomech.* **28** (2004), no. 4, p. 323-337.

[35] R. Verdugo, K. Ishihara, "The steady state of sandy soils", *Soil Found.* **36** (1996), p. 81-91.

[36] K. Ishihara, "Liquefaction and flow failure during earthquakes", *Géotechnique* **43** (1996), no. 3, p. 351-415.

[37] Y. P. Yao, L. Liu, T. Luo, "UH model for sands (in Chinese)", *Chinese J. Geotech. Eng.* **38** (2016), p. 2147-2153.